Lactate dehydrogenase activity drives hair follicle stem cell activation

HHS Public Access

Author manuscript

Nat Cell Biol. Author manuscript; available in PMC 2018 February 14.

Published in final edited form as:

Nat Cell Biol. 2017 September ; 19(9): 1017–1026. doi:10.1038/ncb3575.

Lactate dehydrogenase activity drives hair follicle stem cell activation

Flores Aimee[1,3,4], **Schell John**[10], **Krall Abby**[6], **Jelinek David**[1], **Miranda Matilde**[1], **Grigorian Melina**[14], **Braas Daniel**[6,13], **C White Andrew**[7], **Zhou Jessica**[9], **Graham Nick**[6,9], **Graeber Thomas**[6], **Seth Pankaj**[15], **Evseenko Denis**[8], **Coller Hilary**[1,2,3,4,5], **Rutter Jared**[10,11], **Christofk Heather**[2,3,5,6,13,*], and **E Lowry William**[1,2,3,4,*]

[1]Department of Molecular Cell and Developmental Biology, UCLA

[2]Jonsson Comprehensive Cancer Center, UCLA

[3]Eli and Edythe Broad Center for Regenerative Medicine, UCLA

[4]Molecular Biology Institute, UCLA

[5]Department of Biological Chemistry, UCLA

[6]Department of Molecular and Medical Pharmacology, UCLA

[7]School of Veterinary Medicine, Cornell University

[8]Broad Center for Regenerative Medicine, University of Southern California

[9]Mork Family Department of Chemical Engineering, University of Southern California

[10]Department of Biochemistry, University of Utah

[11]Howard Hughes Medical Institute

[12]Crump Institute for Molecular Imaging, UCLA

[13]UCLA Metabolomics Center, UCLA

[14]Stanford School of Medicine, UCLA

[15]Division of Interdisciplinary Medicine and Biotechnology, Beth Israel Deaconess Cancer Center, Harvard Medical School

Summary

*To whom correspondence should be addressed: William Lowry, blowry@ucla.edu, 310-794-5175 and Heather Christofk, HChristofk@mednet.ucla.edu, 310-794-4248.

Normalized metabolite data is available at figshare.com (https://figshare.com/s/e2d8445b3ec37b5f2c33).

Potential Competing Interest Statement The use of RCGD423 to promote hair growth is covered by a provisional patent application filed by UC Regents and this technology has been licensed by Carthronix LLC. William Lowry is a member of the board of advisors and a shareholder of Carthronix LLC. None of the work in this study was supported by Carthronix. The use of UK5099 to promote hair growth is covered by a separate provisional patent filed by UC Regents with Drs. Lowry and Christofk as inventors.

All other data supporting the findings of this study are available from the corresponding author on reasonable request.

While normally dormant, Hair Follicle Stem Cells (HFSCs) quickly become activated to divide during a new hair cycle. The quiescence of HFSCs is known to be regulated by a number of intrinsic and extrinsic mechanisms. Here we provide several lines of evidence to demonstrate that HFSCs utilize glycolytic metabolism and produce significantly more lactate than other cells in the epidermis. Furthermore, lactate generation appears to be critical for the activation of HFSCs as deletion of lactate dehydrogenase (Ldha) prevented their activation. Conversely, genetically promoting lactate production in HFSCs through mitochondrial pyruvate carrier (Mpc1) deletion accelerated their activation and the hair cycle. Finally, we identify small molecules that increase lactate production by stimulating Myc levels or inhibiting Mpc1 carrier activity and can topically induce the hair cycle. These data suggest that HFSCs maintain a metabolic state that allow them to remain dormant and yet quickly respond to appropriate proliferative stimuli.

Introduction

The hair follicle is able to undergo cyclical rounds of rest (telogen), regeneration (anagen), and degeneration (catagen). The ability of the hair follicle to maintain this cycle depends on the presence of the hair follicle stem cells, which reside in the bulge (Fig 1). At the start of anagen, bulge stem cells are activated by signals received from the dermal papilla, which at that stage abuts the bulge area [1,2]. These stem cells exit the bulge and proliferate downwards, creating a trail that becomes the outer root sheath (ORS). Bulge stem cells are capable of giving rise to all the different cell types of the hair follicle. The ability of HFSCs to maintain quiescence and yet become proliferative for a couple days before returning to quiescence is unique in this tissue, and the precise mechanism by which these cells are endowed with this ability is not fully understood. While significant effort has produced a wealth of knowledge on both the transcriptional and epigenetic mechanisms by which HFSCs are maintained and give rise to various lineages [3,4], little is known about metabolic pathways in the hair follicle or adult stem cells *in vivo*.

Considering the fact that there are essentially no published data on metabolic states of any cell in the hair follicle, a detailed study of metabolism was necessary to understand the nature of HFSCs and their progeny. Several previous studies employed genetic disruption of the mitochondrial electron transport chain in the epidermis by deletion under the control of a pan-epidermal keratin promoter and found that mitochondrial function was essential for maintenance of the follicle[5–8]. However, these studies did not explore the metabolic requirements for specific cell types within the tissue, nor did they explore a role for glycolytic metabolism. In this study, we present methods to study the metabolism of HFSCs *in vivo*, and provide evidence that these cells take advantage of a distinct mode of metabolism not found in their progeny. In the process, we also define small molecules that can take advantage of the unique metabolism of HFSCs to ignite the hair cycle in otherwise quiescent follicles.

Results

Numerous studies have uncovered unique gene expression signatures in HFSCs versus other follicle cells or cells of the interfollicular epidermis [9–12]. Many of these signatures are

regulated by transcription factors that were later shown to play important roles in HFSC homeostasis[13]. Lactate dehydrogenase is most commonly encoded by the *Ldha* and *Ldhb* genes in mammals, the protein products of which form homo- or hetero-tetramers to catalyze the NADH-dependent reduction of pyruvate to lactate and NAD^+-dependent oxidation of lactate to pyruvate[14]. By immunostaining, Ldha appeared to be enriched in quiescent HFSCs *in situ* (telogen) (Fig 1a), IHC with an antibody that recognizes both Ldha and Ldhb showed that only Ldha appears to be localized to the HFSC niche (Supplementary Figure 1a).

HFSCs are known to go through successive rounds of quiescence (telogen) punctuated by brief periods of proliferation correlating with the start of the hair cycle (telogen-anagen transition) [4,15]. Proliferation or activation of HFSCs is well known to be a prerequisite for advancement of the hair cycle. IHC analysis also showed Ldha expression was enriched in HFSCs (Sox9+) at three stages of the hair cycle (Fig 1a). Consistently, immunoblotting of lysates from sorted cells showed strong expression of Ldha in the basal HFSCs (α6HiCD34+), and suprabasal (α6LoCD34+) HFSC populations relative to total epidermis (Fig 1b)[9] (Sorting strategy is outlined in Supplementary Figure 1b).

To determine whether Ldha expression patterns correlate with activity of the Ldh enzyme, we used a colorimetric-based enzymatic assay to assess Ldh activity capacity *in situ*. Typically performed on protein lysates or aliquots with a plate reader[16], we adapted the Ldh activity assay to work *in situ* on frozen tissue sections. Note that since both the *in situ* and *in vitro* Ldh activity assays employ use of excess substrate (lactate), the results from these assays reflect the capacity for Ldh activity, and not the steady-state activity.

Applying this assay to skin samples demonstrated that Ldh activity capacity was significantly higher in HFSCs, consistent with the expression pattern of Ldha (Fig 1c). Furthermore, Ldh activity was enriched in HFSCs across the hair cycle (Fig 1c). As a control, assays conducted without the enzymatic substrate (lactate) or on acid-treated tissue yielded zero activity (Supplementary Figure 1c). To further validate these results, we sorted epidermal populations, generated cell lysates on the sorted cells, and performed a similar colorimetric-based enzymatic assay on the sorted cell lysates, which also showed increased Ldh activity in HFSCs (Fig 1d). To better characterize the metabolism of HFSCs, we performed metabolomics analysis on sorted populations from mouse skin by liquid chromatography-mass spectrometry (LC-MS) (Fig 1e). Several glycolytic metabolites, including glucose/fructose-6-phosphate, fructose-bisphosphate, dihydroxyacetone phosphate, 3-phosphoglycerate, and lactate, were routinely higher in HFSCs relative to total epidermis across three independent experiments (isolated from different mice on different days). Conversely, most TCA cycle metabolites were not consistently different between the epidermis and HFSCs (Fig 1e). Collectively these results suggest that while all cells in the epidermis use the TCA cycle extensively to generate energy, HFSCs also have increased Ldha expression, Ldh activity, and glycolytic metabolism.

Measuring metabolism across the hair cycle therefore would capture any dynamic changes that occur in HFSCs that correlate with activation or quiescence. Analysis of RNA-seq data from HFSCs isolated during either telogen or the telogen-anagen transition demonstrated not

only that *Ldha* is the predominant *Ldh* isoform expressed in HFSCs (Fig 2c), but is also induced during the telogen-anagen transition (Fig 2a and b (NIHGEOGSE67404 and GSE51635). To confirm that the cells analyzed by RNA-seq were indeed either in telogen or the telogen to anagen transition, important markers of this transition were assessed including the Shh and Wnt pathways (*Gli1, 2, 3; Lef1, Axin1, Axin2, Ccnd1*) as well as proliferation markers (*Ki-67, Pcna and Sox4*) (Supplementary Figure 2a).

The *in vitro* Ldh activity assay on lysates from sorted HFSCs uncovered a modest induction of Ldh activity correlating with the telogen to anagen transition (Fig 2d). Hair cycle staging was validated by Ki-67 immunostaining to determine HFSC activation (Supplementary Figure 2b). Additionally, measurements of steady-state metabolites extracted from sorted HFSCs showed an increase in lactate in HFSCs as they transition from telogen to telogen-anagen transition, and then decrease again in anagen as HFSCs return to quiescence (Fig 2e).

To determine whether Ldh activity is functionally related to the ability of HFSCs to remain quiescent or to activate at the start of a hair cycle, we deleted *Ldha* specifically in the HFSCs. Taking advantage of mice with floxed alleles of *Ldha*[17], this enzyme was deleted in HFSCs by crossing to mice bearing the *K15CrePR* allele[11], known to be inducible by Mifepristone specifically in HFSCs. Deletion of *Ldha* in HFSCs was initiated by administration of Mifepristone during telogen (day 50) and led to a typically mosaic recombination of the floxed alleles across the backskin[11,18]. Mice with HFSC-specific deletion of *Ldha* failed to undergo a proper hair cycle, with most follicles remaining in telogen across at least 33 pairs of littermates 3–4 weeks after Mifepristone treatment (Fig 3a). A complete list of transgenic animals including birthdate, sex, and genotype is provided in Supplemental Table 1.

Histology showed that WT hair follicles entered into the telogen to anagen transition typically by day 70, and this was accompanied by typical expansion of the hypodermis below (Fig 3b). However, in backskin with deletion of *Ldha*, the hypodermis did not expand, and the telogen to anagen transition was severely abrogated (Fig 3b). In areas of strong phenotypic penetrance, Ldh activity was severely abrogated in the HFSC compartment (Fig 3c), demonstrating that the *Ldha* allele is critically important for Ldh activity in HFSCs and consistent with the fact that the ‘a’ isoform of *Ldh* is expressed at the highest level. Quantification of hair cycle progression across numerous animals indicated that most follicles lacking *Ldha* remained in telogen (Fig 3d).

In addition, to confirm the phenotypes, we also deleted *Ldha* with an independent HFSC-specific Cre strategy. *Lgr5-CreER* has been used for lineage tracing in a variety of adult stem cell models, and has been shown to mark cells with high regenerative capacity, including HFSCs[19]. *Lgr5CreER;Ldha*$^{fl/fl}$ mice, treated with tamoxifen at post-natal day 50 prior to a synchronized hair cycle, also failed to activate anagen across at least 20 littermate pairs (Fig 3g). *in situ* Ldh assay and metabolomics confirmed the successful deletion of *Ldha* in these animals (Fig 3h and 3i).

We also monitored the effect of loss of Ldha activity in K15+ cells over a six month period and found that deletion of *Ldha* led to a mosaic, but permanent block of HFSC activation in some portions of the backskin (Supplementary Figure 3a). These data confirm that Ldh activity is required for HFSC activation, and is not simply a marker of HFSCs. A closer look at these long term *Ldha* deletions showed that *Ldha*-null HFSCs continued expressing typical markers, but lacked Ldh activity, and failed to initiate new hair cycles, while those follicles that escaped deletion continued to express Ldha and to cycle normally (Supplementary Figure 3b and c).

After sorting HFSCs from animals with or without *Ldha* deletion, LC-MS-based metabolomics analysis demonstrated that lactate levels, as well as levels of other glycolytic metabolites, were strongly reduced in the absence of Ldha (Fig 3e), functional evidence that the targeting strategy was successful. The fact that glycolytic metabolites upstream of lactate were also suppressed suggests that HFSCs could be adapting their metabolism to account for the loss of Ldh activity. Immunostaining for markers of HFSC activation and proliferation indicated a failure of HFSC activation. Ki67 and pS6 have been clearly demonstrated to be abundant in the HFSC niche at the start of the hair cycle[20], and both of these markers were absent in *Ldha* deleted backskin (Fig 3f). Immunostaining for Ldha also confirmed successful deletion of this protein, while staining for Sox9, a marker of HFSCs indicated that these cells remained in their niche, but just failed to activate in the absence of Ldha (Fig 3f). Induction of the hair cycle is also thought to be regulated by signaling from the Shh, Wnt and Jak-Stat pathways. We assayed each of these by IHC in normal or *Ldha* deletion follicles and found that in general these pathways were not activated in *Ldha*-null HFSCs that failed to enter a telogen-anagen transition (Supplementary Figure 3d).

To determine whether induction of lactate production could affect HFSC activation or the hair cycle, we crossed *K15CrePR* animals to those floxed for mitochondrial pyruvate carrier 1 (*Mpc1*) (*K15CrePR;Mpc1*$^{fl/fl}$). Mpc1, as a heterodimer with Mpc2, forms the mitochondrial pyruvate carrier MPC, a transporter on the inner mitochondrial membrane required for pyruvate entry into the mitochondria[21]. Loss of function of Mpc1 has been shown to drive lactate production through enhanced conversion of pyruvate to lactate by Ldh [22].

In animals with *Mpc1* deletion in HFSCs, we observed a strong acceleration of the ventral and dorsal hair cycles with all the typical features of a telogen-anagen transition (Fig 4a) (n = 12 littermate pairs). Mifepristone treated *K15CrePR;Mpc1*$^{fl/fl}$ animals were the only to show any signs of dorsal anagen by day 70. Western blotting on sorted HFSCs validated the loss of Mpc1 protein (Fig 4b). Importantly, purified HFSCs lacking *Mpc1* showed a strong induction of Ldh activity (Fig 4c). Quantification of the dorsal hair cycle across three pairs of littermates showed a strong induction of anagen in backskin lacking *Mpc1* (Fig 4d, right), and histology showed that the anagen induction was normal in appearance with a typical hypodermal expansion (Fig 4d). Immunostaining demonstrated the induction in *Mpc1-null* HFSCs of various markers of hair cycle activation such as Ki-67 and pS6, while Sox9 expression was unaffected (Fig 4e). Long term deletion of *Mpc1* did not lead to aberrant follicles or exhaustion of HFSCs as judged by pathology and staining for Sox9 (Supplementary Figure 4a). Furthermore, deletion of *Mpc1* with *Lgr5CreER* showed a very

similar phenotype as deletion with *K15CrePR* (Fig 4f and g), validating the fact that deletion of this protein in HFSCs leads to their activation (n = 12 pairs of littermates). Finally, immunofluorescence for the *Ires-GFP* of the *Lgr5CreER* transgene along with Ki-67 and lineage tracing with K15CrePR;Mpc1$^{fl/fl}$;lsl-Tomato mice also demonstrated that the HFSCs were indeed proliferative following induction of Mpc1 deletion by tamoxifen or mifepristone (Supplementary Figure 4b).

On the other hand, deletion of *Mpc1* in the top of the follicle (infundibulum, sebaceous gland progenitors) and a limited number of interfollicular cells with *Lgr6CreER* [23] did not appear to affect the hair cycle (*Lgr6CreER;Mpc1$^{fl/fl}$*) (n = 10 littermate pairs) or general skin homeostasis over at least 2 months (Fig S4c). Ldh activity assay on Lgr6+ cells sorted from wildtype or deletion skin demonstrated that the *Mpc1* deletion was effective (Supplementary Figure 4d). Together, these results indicate that increasing lactate production through the blockade of pyruvate into the TCA cycle has a strong effect on the ability of HFSCs, but not other cells in the hair follicle, to become activated to initiate a new hair cycle.

UK-5099 is a well-established pharmacological inhibitor of the mitochondrial pyruvate carrier and is known to promote lactate production as a result in various settings[24]. Topical treatment of animals in telogen (day 50) with UK-5099 led to a robust acceleration of the hair cycle, as well as minor hyperproliferation of the interfollicular epidermis (Fig 5a). Quantification of the hair cycle across at least 6 pairs of animals (vehicle vs UK-5099) indicated a strong acceleration of the hair cycle, in as few as 6–9 days (Fig 5b). Similar to genetic deletion of *Mpc1*, pharmacological blockade of the mitochondrial pyruvate carrier by UK-5099 for 48 hours during telogen promoted increased Ldh activity in HFSCs and the interfollicular epidermis, consistent with increased capacity for lactate production (Fig 5c). Finally, metabolomic analysis demonstrated that topical application of UK-5099 increases total levels of lactate in sorted HFSCs (Fig 5d).

Because alteration of lactate production in HFSCs appeared to regulate their activation, we attempted to identify other small molecules that could take advantage of these findings to induce the hair cycle. *Ldha* is known to be transcriptionally regulated by Myc, which has been shown to play an important role in HFSC activation and the hair cycle[25–27]. RNA-seq on sorted HFSCs indicated that Myc is induced during the telogen-anagen transition (Fig 6a). Western blotting for both c-Myc and n-Myc in sorted HFSCs versus total epidermis showed a strong increase in Myc protein in the nuclei of HFSCs (Fig 6b).

Taking advantage of a molecule with the robust ability to promote Myc expression through binding of GP130 and activation of Jak/Stat signaling, we topically treated mice for 48 hours to determine the effect of RCGD423 on Stat signaling and Myc expression. We found that RCGD423 induced levels of both c-Myc and n-Myc as well as Ldha (Fig 6c), consistent with activation of Stat3 signaling leading to induction of Myc and Ldha protein expression. *In vitro* measurement of Ldh activity on lysates from total epidermis showed an increase in activity by RCGD423 (Fig 6d). *In situ* staining for Ldh activity showed a strong induction upon treatment with RCGD423 in both the epidermis and even in the dermis, as expected with topical treatment (Fig 6e). LC-MS-based metabolomics on epidermis isolated from

vehicle or RCGD423 showed a large increase in lactate as well, even after just 48 hours (Fig 6f).

RCGD423 binds to GP130, a co-receptor for Jak-Stat signaling, and activates Stat-3. We found that Stat-3 was activated in HFSCs by RCGD423 after topical treatment by immunostaining with phospho-Stat3 antibody (Fig 6g). This also correlated with induction of Ki-67 in HFSCs in the same tissue (Fig 6g). IHC for pStat1 and pStat5 suggested that RCGD423 does not dramatically affect these other Stat family members (Supplementary Figure 5). Topical treatment of animals in telogen (day 50) with RCGD423 led to a robust acceleration of the hair cycle (Fig 6h), as well as minor hyperproliferation of the interfollicular epidermis.

Discussion

Together, these data demonstrate that the production of lactate, through Ldha, is important for HFSC activation, and that HFSCs may maintain a high capacity for glycolytic metabolism at least in part through the activity of Myc. Our data also demonstrate that a genetic or pharmacological disruption of lactate production can be exploited to regulate the activity of HFSCs. It is possible that these results have implications for adult stem cells in other tissues. In an accompanying manuscript, the Rutter lab describes a role for Mpc1 in adult intestinal stem cells[28]. Consistent with data presented here on HFSCs, deletion of Mpc1 led to an increase in the ability of intestinal stem cells to form organoids.

Previous work showed that hematopoietic stem cells (HSCs) show higher glycolytic activity, but disruption of glycolysis in the HSCs led to activation of their cycling[29–32], contrary to what we find with HFSCs. While the distinction could be biological, there are technical reasons for potential discrepancies as well. First, there are no Cre transgenic lines that can delete genes specifically in HSCs, as opposed to HFSCs (K15+ or Lgr5+). Second, to block glycolysis in HSCs, the previous study deleted PDK enzyme, which would only indirectly regulate glycolysis, whereas here we deleted Ldh enzyme specifically. In addition, HSCs and HFSCs are functionally distinct in that HFSCs only cycle at well-defined moments (telogen to anagen transition), while the timing of HSC activation is not as well established or synchronized. Instead, we hypothesize that increased glycolytic rate in HFSCs allows them to respond quickly to the barrage of cues that orchestrate the onset of a new hair cycle. This has also been proposed to be the case for neural stem cells based solely on RNA-seq data[33], but as of yet no *in vivo* functional evidence exists to confirm this possibility.

The fact that small molecules could be used to promote HFSC activation suggests that they could be useful for regenerative medicine. This is not only the case for hair growth, but potentially for wound healing as well. While HFSCs do not normally contribute to the interfollicular epidermis, in a wound setting, HFSCs migrate towards the wound site and make a contribution, as measured by lineage tracing[34]. Whether activation of Ldh enzyme activity by Mpc1 inhibition (UK-5099) or Myc activation (RCGD423) can promote wound healing will be the subject of intense effort going forward.

Materials and Methods

Mice

Several of the animal strains came from Jackson Labs (*K15-CrePR*, *Lgr5-CreER* and *Lgr6-CreER*), while others were generated in the Rutter (*Mpc*$^{fl/fl}$) and Seth Labs[36] (*Ldha*$^{fl/fl}$) and maintained under conditions set forth by IUCUC and UCLA ARC. For experiments that include analysis of the telogen stage of the hair cycle, animals were harvested at post-natal day 50, for telogen-anagen transition animals were harvested at day 70, and for anagen animals were harvested at post-natal day 90. For experiments that include analysis of transgenic animals, *K15-CrePR* animals were shaved and treated by injection of mifepristone and *Lgr5-CreER* and *Lgr6-CreER* animals were shaved and treated with tamoxifen (10 mg/ml dissolved in sunflower seed oil, 2 mg per day for 3 days) during telogen (post-natal day 50), and monitored for hair regrowth following shaving. For Figs. 5 and 6, wildtype C57BL/6J animals were shaved at post-natal day 50 and treated topically with Transderma Plo Gel Ultramax Base (TR220) (vehicle), UK-5099 (Sigma PZ0160) (20uM) or RCGD423 (50uM) for indicated periods of time. Both male and female animals were used in this study in approximately equal numbers with no apparent difference in phenotype between genders. All animal experiments were done in compliance with ethical guidelines and approved by the UCLA Animal Research Committee (ARC) according to IACUC guidelines in facilities run by the UCLA Department of Laboratory Animal Medicine (DLAM).

Histology, Immunostaining and Immunoblotting

Tissues were isolated from the indicated genotypes and embedded fresh in OCT compound for frozen tissue preparations, or fixed overnight in 4% formalin and embedded in paraffin. For frozen tissue, sectioning was performed on a Leica 3200 Cryostat, and fixed for 5 minutes in 4% paraformaldehyde. Paraffin embedded tissue was sectioned, de-paraffinized, and prepared for histology. All sections prepared for staining were blocked in staining buffer containing appropriate control IgG (Goat, Rabbit etc.). Immunohistochemistry was performed on formalin-fixed paraffin-embedded tissue with citrate or Tris buffer antigen retrieval with the following antibodies: Ki67 (Abcam ab16667, 1:50), p-S6 (Cell Signaling CST2215, 1:50), Sox9 (Abcam ab185230, 1:1000), Ldha (Abcam ab47010, 1:100), Ldh (Abcam ab125683, 1:100), p-Stat3 (Abcam ab68153, 1:200), p-Stat1 (Abcam ab109461, 1:200), p-Stat5 (Abcam ab32364; 1:50), Gli3 (Abcam ab6050; 1:100), β-catenin (Abcam ab32572; 1:500). The DAKO EnVision+ HRP Peroxidase System (Dako K400911-2) and Dako AEC Substrate Chromogen (Dako K346430-2) was used for detection. Images were collected on an Olympus BX43 Upright Microscope and Zeiss Model Axio Imager M1 Upright Fluorescence Microscope. Protein samples for western blots and enzymatic assays were extracted from FACS sorted epidermal populations in RIPA lysis buffer (Pierce) with Halt protease and phosphatase inhibitors (Thermo-Fisher) and precipitated in acetone for concentration. The following antibodies were used: β-actin (Abcam ab8227; 1:1000), β-actin (Santa Cruz sc-47778; 1:1000), C-Myc (Abcam ab32072; 1:1000), N-Myc (Santa Cruz sc-53993; 1:200), H3K27Ac (Abcam ab177178; 1:200), Mpc1(Sigma HPA045119).

Cell isolation and FACS

Whole dorsal and ventral mouse skin were excised and floated on trypsin (0.25%) for 1 h at 37° or overnight at 4°. The epidermis was separated from dermis by scraping and epidermal cells were mechanically dissociated using a pipette. Epidermal cells were filtered with a 70 μM cell strainer into 20% BCS, collected at 300g and washed twice with PBS. The cells were then filtered through a 40 μM cell strainer and stained for FACS processing with CD34 Monoclonal Antibody (RAM34), FITC, eBioscience™ (Catalog #:11-0341-82) and CD49d (Integrin alpha 4) Monoclonal Antibody (R1-2), PE, eBioscience™ (Catalog #:12-0492-81). Gating strategy shown in Suppl Fig 1b. Cells sorted using BD FACSAria high-speed cell sorters. Single positive and double positive populations were collected into 20% BCS, RIPA lysis buffer (Thermo Scientific, Pierce), or 80% methanol for enzymatic assays, western blots or mass spec analyses respectively.

Cell lines

No cell lines were used in this study.

Plate-reader Ldh assay

Ldh activity was determined in cell lysates by measuring the formation of soluble XTT formazan in direct relation to production of NADH over time at 475 nm at 37°C using a Synergy-MX plate reader (Biotek Instruments). Lysates were prepared in RIPA Buffer (Thermo Scientific Pierce). Protein content was determined using the BCA Protein Assay Kit (Thermo Scientific Pierce). 10 μg of protein were used per well. The staining solution contained 50 mM Tris buffer pH 7.4, 150 μM XTT (Sigma), 750 μM NAD (Sigma), 80 μM phenazine methosulfate (Sigma) and 10mM of substrate lactate (Sigma). Ldh activity was determined in cell lysates by measuring the change in absorbance of their common substrate or product, NADH, over time at 340 nm at 25°C using a Synergy-MX plate reader (Biotek Instruments).

In situ Ldh assay

Cryostat sections of mouse skin were briefly fixed (4% formalin for 5 min), washed with PBS pH 7.4, and then incubated with the appropriate solution for LDH activity. Staining medium contained 50 mM Tris pH 7.4, 750 μM NAD (Sigma), 80 μM phenazine methosulfate (Sigma), 600 μM Nitrotetrazolium Blue chloride (Sigma), 10 mM $MgCl_2$ (Sigma) and 10mM of the substrate lactate (Sigma). Slides were incubated with staining medium at 37°C until they reached the desired intensity, then counterstained using Nuclear Fast Red (Vector, Burlingame, CA) and mounted using VectaMount (Vector, Burlingame, CA). Control reactions were performed by using incubation medium that lacked the substrate mixture or NAD.

Mass spectrometry-based metabolomics analysis

The experiments were performed as described in [36]. To extract intracellular metabolites, FACS sorted cells were briefly rinsed with cold 150 mM ammonium acetate (pH 7.3), followed by addition of 1 ml cold 80% MeOH on dry ice. Cell suspensions were transferred into Eppendorf tubes and 10 nmol D/L-norvaline was added. After rigorously mixing, the

suspension was pelleted by centrifugation ($1.3*10^4$ rpm, 4 °C). The supernatant was transferred into a glass vial, metabolites dried down under vacuum, and resuspended in 70% acetonitrile. For the mass spectrometry-based analysis of the sample, 5 ul was injected onto a Luna NH2 (150 mm × 2 mm, Phenomenex) column. The samples were analyzed with an UltiMate 3000RSLC (Thermo Scientific) coupled to a Q Exactive mass spectrometer (Thermo Scientific). The Q Exactive was run with polarity switching (+3.50 kV / −3.50 kV) in full scan mode with an m/z range of 65–975. Separation was achieved using A) 5 mM NH_4AcO (pH 9.9) and B) ACN. The gradient started with 15% A) going to 90% A) over 18 min, followed by an isocratic step for 9 min and reversal to the initial 15% A) for 7 min. Metabolites were quantified with TraceFinder 3.3 using accurate mass measurements (≤ 3 ppm) and retention times. Normalized metabolite data is available at figshare.com (https://figshare.com/s/e2d8445b3ec37b5f2c33).

Statistics and Reproducibility

Experiments were performed on male and female animals in approximately equal numbers with no apparent difference in phenotype between sexes. All phenotypes described are representative of a minimum of n = 3 littermate pairs as indicated in the description of each experiment. For analysis of the hair regrowth phenotype no statistical measure was used to determine the sample size beforehand, nor were statistics used to measure effects, as the results were essentially positive or negative as represented in the figures. The results described include data from all treated animals. Investigators were not blinded to allocation during the experimental data collection. Experiments were not randomized. All results shown were representative images from at least three independently treated animals, and genotyping was performed both before and after animal treatment for confirmation. For graphs, all comparisons are shown by Student's two-tailed unpaired t-test and all graphs, bars or lines indicate mean and error bars indicate Standard error of the mean (s.e.m).

Data Availability

Previously published transcriptomics data that were re-analysed here are available under accession code GSE67404 and 51635[37,38].

Supplementary Material

Refer to Web version on PubMed Central for supplementary material.

Acknowledgments

We would like to acknowledge the significant technical support of Mallory Neebe, Jessica Cinkornpumin, and Anqi Liu on this project. We are also particularly grateful to members of the Banerjee lab for guidance and development of the Ldh activity assay. AF and ACW were supported by a fellowship from the Eli and Edythe Broad Center for Regenerative Medicine at UCLA. ACW and MG were supported by a fellowship from the Tumor Cell Biology program at UCLA (NIH). ACW was also supported by a training grant from CIRM. DJ was supported by awards from a New Idea Award from the Leukemia Lyphoma Society, the Jonsson Comprehensive Cancer Center, the UCLA Clinical Translational Science Institute UL1TR000124, the Prostate Cancer SPORE at UCLA P50 CA092131, and the Eli & Edythe Broad Center for Regenerative Medicine & Stem Cell Research. NAG is a postdoctoral trainee supported by the UCLA Scholars in Oncologic Molecular Imagining program (NCI/NIH grant R25T CA098010). AK was supported by a UCLA Dissertation Year Fellowship. HAC was supported by National Institute of General Medical Sciences R01-GM081686 and R01-GM0866465. JR was supported by NIH (RO1GM094232) HRC was supported by a Research Scholar Grant, RSG-16-111-01-MPC, from the American Cancer Society and the Eli & Edythe Broad Center of Regenerative Medicine and Stem Cell Research at UCLA and

Rose Hills Foundation Research Award. WEL was supported by NIH-NIAMS (5R01AR57409), an Impact award from CTSI and the Jonsson Comprehensive Cancer Foundation, and The Gaba Fund through the Eli & Edythe Broad Center of Regenerative Medicine at UCLA.

References

1. Hsu YC, Pasolli HA, Fuchs E, et al. Dynamics between stem cells, niche, and progeny in the hair follicle. Cell. 2011; 144:92–105. DOI: 10.1016/j.cell.2010.11.049 [PubMed: 21215372]
2. Morris RJ, Potten CS. Highly persistent label-retaining cells in the hair follicles of mice and their fate following induction of anagen. J Invest Dermatol. 1999; 112:470–475. [PubMed: 10201531]
3. Fuchs E, et al. The tortoise and the hair: slow-cycling cells in the stem cell race. Cell. 2009; 137:811–819. DOI: 10.1016/j.cell.2009.05.002 [PubMed: 19490891]
4. Fuchs E, Merrill BJ, Jamora C, DasGupta R. At the roots of a never-ending cycle. Dev Cell. 2001; 1:13–25. [PubMed: 11703920]
5. Kloepper JE, et al. Mitochondrial function in murine skin epithelium is crucial for hair follicle morphogenesis and epithelial-mesenchymal interactions. J Invest Dermatol. 2015; 135:679–689. DOI: 10.1038/jid.2014.475 [PubMed: 25371971]
6. Hamanaka RB, Chandel NS, et al. Mitochondrial metabolism as a regulator of keratinocyte differentiation. Cell Logist. 2013; 3:e25456. [PubMed: 24475371]
7. Hamanaka RB, et al. Mitochondrial reactive oxygen species promote epidermal differentiation and hair follicle development. Sci Signal. 2013; 6:ra8. [PubMed: 23386745]
8. Baris OR, et al. The mitochondrial electron transport chain is dispensable for proliferation and differentiation of epidermal progenitor cells. Stem Cells. 2011; 29:1459–1468. DOI: 10.1002/stem.695 [PubMed: 21780252]
9. Blanpain C, Lowry WE, Geoghegan A, Polak L, Fuchs E. Self-renewal, multipotency, and the existence of two cell populations within an epithelial stem cell niche. Cell. 2004; 118:635–648. [PubMed: 15339667]
10. Tumbar T, et al. Defining the epithelial stem cell niche in skin. Science. 2004; 303:359–363. [PubMed: 14671312]
11. Morris RJ, et al. Capturing and profiling adult hair follicle stem cells. Nat Biotechnol. 2004; 22:411–417. [PubMed: 15024388]
12. Trempus CS, et al. Enrichment for living murine keratinocytes from the hair follicle bulge with the cell surface marker CD34. J Invest Dermatol. 2003; 120:501–511. [PubMed: 12648211]
13. Nguyen H, Rendl M, Fuchs E. Tcf3 governs stem cell features and represses cell fate determination in skin. Cell. 2006; 127:171–183. [PubMed: 17018284]
14. Fromm HJ. The nature of pyruvate involved in the enzymic formation of L-lactate in the rabbit-muscle lactate dehydrogenase reaction. Biochim Biophys Acta. 1965; 99:540–542. [PubMed: 4284664]
15. Paus R, Muller-Rover S, Botchkarev VA. Chronobiology of the hair follicle: hunting the “hair cycle clock”. J Investig Dermatol Symp Proc. 1999; 4:338–345.
16. Chan FK, Moriwaki K, De Rosa MJ, et al. Detection of necrosis by release of lactate dehydrogenase activity. Methods Mol Biol. 2013; 979:65–70. DOI: 10.1007/978-1-62703-290-2_7 [PubMed: 23397389]
17. Xie H, et al. Targeting lactate dehydrogenase--a inhibits tumorigenesis and tumor progression in mouse models of lung cancer and impacts tumor-initiating cells. Cell Metab. 2014; 19:795–809. DOI: 10.1016/j.cmet.2014.03.003 [PubMed: 24726384]
18. White AC, et al. Defining the origins of Ras/p53-mediated squamous cell carcinoma. Proc Natl Acad Sci U S A. 2011; 108:7425–7430. 1012670108 [pii]. DOI: 10.1073/pnas.1012670108 [PubMed: 21502519]
19. Jaks V, et al. Lgr5 marks cycling, yet long-lived, hair follicle stem cells. Nat Genet. 2008; 40:1291–1299. ng.239 [pii]. DOI: 10.1038/ng.239 [PubMed: 18849992]
20. Kellenberger AJ, Tauchi M, et al. Mammalian target of rapamycin complex 1 (mTORC1) may modulate the timing of anagen entry in mouse hair follicles. Exp Dermatol. 2013; 22:77–80. DOI: 10.1111/exd.12062 [PubMed: 23278901]

21. Bricker DK, et al. A mitochondrial pyruvate carrier required for pyruvate uptake in yeast, Drosophila, and humans. Science. 2012; 337:96–100. DOI: 10.1126/science.1218099 [PubMed: 22628558]
22. Schell JC, et al. A role for the mitochondrial pyruvate carrier as a repressor of the Warburg effect and colon cancer cell growth. Mol Cell. 2014; 56:400–413. DOI: 10.1016/j.molcel.2014.09.026 [PubMed: 25458841]
23. Snippert HJ, et al. Lgr6 marks stem cells in the hair follicle that generate all cell lineages of the skin. Science. 2010; 327:1385–1389. 327/5971/1385 [pii]. DOI: 10.1126/science.1184733 [PubMed: 20223988]
24. Patterson JN, et al. Mitochondrial metabolism of pyruvate is essential for regulating glucose-stimulated insulin secretion. J Biol Chem. 2014; 289:13335–13346. DOI: 10.1074/jbc.M113.521666 [PubMed: 24675076]
25. Wang N, et al. The expression and role of c-Myc in mouse hair follicle morphogenesis and cycling. Acta Histochem. 2012; 114:199–206. DOI: 10.1016/j.acthis.2011.04.009 [PubMed: 21621827]
26. Bull JJ, et al. Ectopic expression of c-Myc in the skin affects the hair growth cycle and causes an enlargement of the sebaceous gland. Br J Dermatol. 2005; 152:1125–1133. DOI: 10.1111/j.1365-2133.2005.06458.x [PubMed: 15948972]
27. Zanet J, et al. Endogenous Myc controls mammalian epidermal cell size, hyperproliferation, endoreplication and stem cell amplification. J Cell Sci. 2005; 118:1693–1704. DOI: 10.1242/jcs.02298 [PubMed: 15797928]
28. JS, JR. Nature Cell Biology. 2017 in press.
29. Hsu P, Qu CK, et al. Metabolic plasticity and hematopoietic stem cell biology. Curr Opin Hematol. 2013; 20:289–294. DOI: 10.1097/MOH.0b013e328360ab4d [PubMed: 23615055]
30. Harris JM, et al. Glucose metabolism impacts the spatiotemporal onset and magnitude of HSC induction in vivo. Blood. 2013; 121:2483–2493. DOI: 10.1182/blood-2012-12-471201 [PubMed: 23341543]
31. Takubo K, et al. Regulation of glycolysis by Pdk functions as a metabolic checkpoint for cell cycle quiescence in hematopoietic stem cells. Cell Stem Cell. 2013; 12:49–61. DOI: 10.1016/j.stem.2012.10.011 [PubMed: 23290136]
32. Simsek T, et al. The distinct metabolic profile of hematopoietic stem cells reflects their location in a hypoxic niche. Cell Stem Cell. 2010; 7:380–390. DOI: 10.1016/j.stem.2010.07.011 [PubMed: 20804973]
33. Shin J, et al. Single-Cell RNA-Seq with Waterfall Reveals Molecular Cascades underlying Adult Neurogenesis. Cell Stem Cell. 2015; 17:360–372. DOI: 10.1016/j.stem.2015.07.013 [PubMed: 26299571]
34. Ito M, et al. Stem cells in the hair follicle bulge contribute to wound repair but not to homeostasis of the epidermis. Nat Med. 2005; 11:1351–1354. [PubMed: 16288281]
35. Wang L, Siegenthaler JA, Dowell RD, Yi R, et al. Foxc1 reinforces quiescence in self-renewing hair follicle stem cells. Science. 2016; 351:613–617. DOI: 10.1126/science.aad5440 [PubMed: 26912704]
36. Xie H, et al. Targeting lactate dehydrogenase--a inhibits tumorigenesis and tumor progression in mouse models of lung cancer and impacts tumor-initiating cells. Cell metabolism. 2014; 19:795–809. [PubMed: 24726384]
37. White AC, et al. Stem cell quiescence acts as a tumour suppressor in squamous tumours. Nat Cell Biol. 2014; 16:99–107. [PubMed: 24335650]
38. Wang L, Siegenthaler JA, Dowell RD, Yi R. Foxc1 reinforces quiescence in self-renewing hair follicle stem cells. Science. 2016; 351:613–7. [PubMed: 26912704]

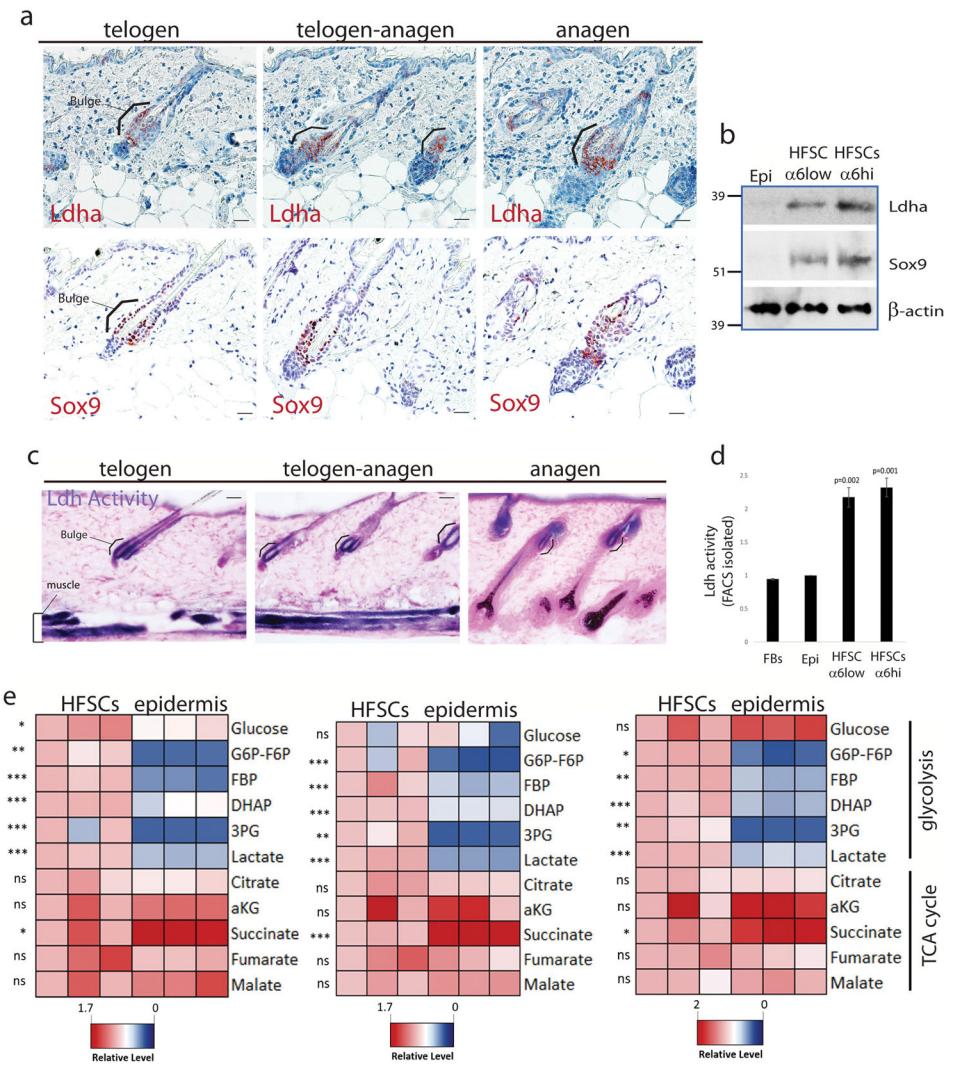

Figure 1. Lactate dehydrogenase activity is enriched in HFSCs

a, IHC staining for Ldha expression across the hair cycle shows Ldha protein confined to the HFSC niche, the bulge, indicated by the bracket. IHC staining for Sox9 on serial sections demarcates the HFSC population. Scale bar indicates 20 micrometers. **b**, Immunoblotting on FACS-isolated HFSC populations (α6low/Cd34+ and α6hiCd34+) versus total epidermis (Epi) shows differential expression of Ldha in the stem cell niche. Sox9 is a marker of HFSCs, and β-actin is a loading control. **c**, Colorimetric assay for Ldh enzyme activity in the epidermis shows highest activity in the bulge (brackets) and subcuticular muscle layer (bracket). This activity is enriched in the bulge across different stages of the hair cycle. Activity is indicated by purple color; pink is a nuclear counterstain. Note also that developing hair shafts in pigmented mice show strong deposits of melanin as observed here; hair shafts never displayed any purple stain indicative of Ldh activity. Scale bars indicate 50 micrometers. **d**, Ldh activity in sorted cell populations, measured using a plate reader-based assay, also shows the highest Ldh activity in two separate HFSC populations (α6hi/Cd34 and α6low/Cd34) compared to epidermal cells (Epi) and fibroblasts (FBs). Each bar

represents the average signal for each cell type where n=9 mice pooled from 3 independent experiments. Shown as mean ± SEM. Paired t-test was performed, $p < 0.05$ shown for each cell type versus epidermal cells **e**, HFSCs and epidermal cells were isolated during telogen (day 50) by FACS, and metabolites were extracted and analyzed by LC-MS. Heatmaps show relative levels of glycolytic and TCA cycle metabolites from cells isolated from different mice in independent experiments with cells from three animals in each. Asterisks indicate significant difference in metabolite levels between epidermal cells and HFSCs. For **e,** paired t-test was performed; * denotes $p < 0.05$, ** denotes $p < 0.01$, *** denotes $p < 0.001$, ns denotes $p > 0.05$, and n=9 mice pooled from 3 independent experiments. Unprocessed scans of blots are shown in Supplementary Figure 6.

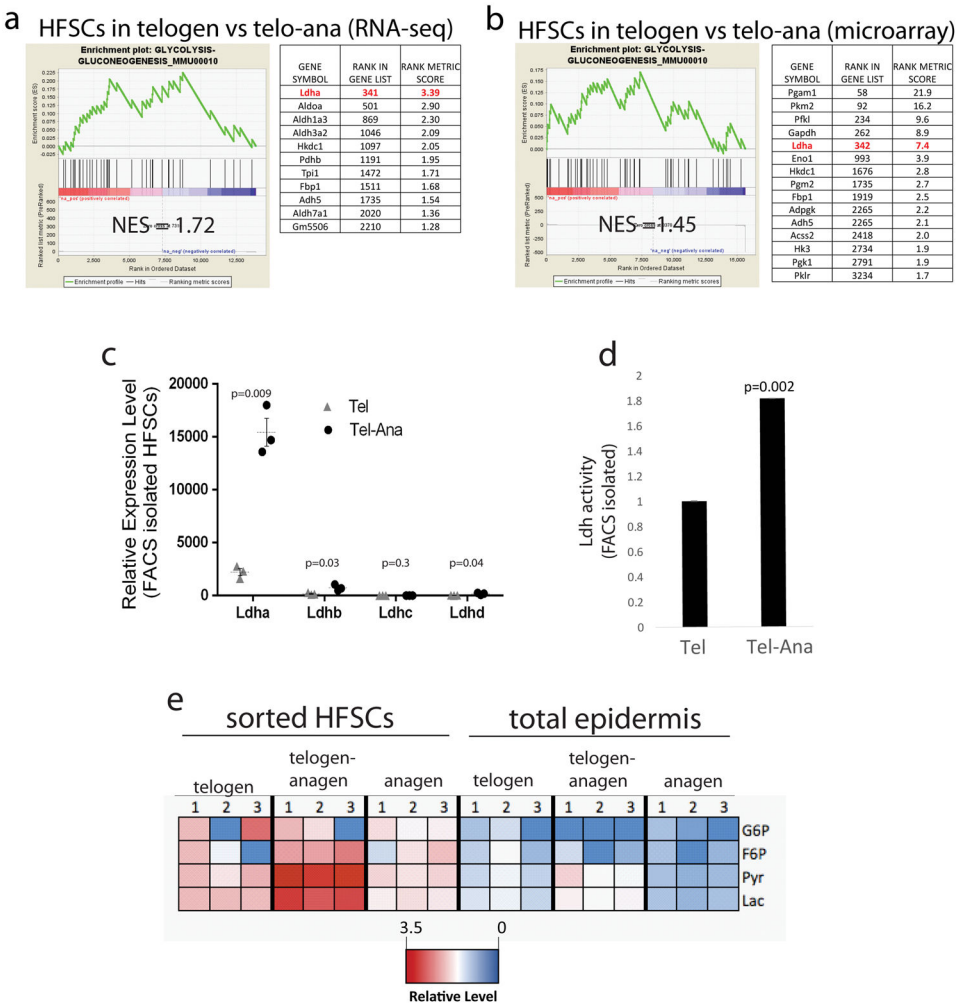

Figure 2. Ldh activity increases during HFSC activation

a, GSEA on RNA-seq transcriptome data from HFSCs versus total epidermis shows enrichment for Glycolysis related genes in HFSCs (NES = 1.72). **b**, GSEA on microarray transcriptome data from HFSCs versus total epidermis shows enrichment for Glycolysis related genes in HFSCs (NES = 1.45). Results were generated from three mice of each condition. **c**, RNA-seq data from HFSCs sorted during telogen or telogen-anagen transition show induction of Ldha[35]. Data represent the average of three separate animals at each timepoint (n = 3), and subjected to students t-test for significance ($p < 0.05$). **d,** Ldh activity in sorted stem cell populations, measured using a plate reader-based assay, shows elevated Ldh activity as stem cells become activated in telogen to anagen transition (Tel-Ana). Each bar represents the average signal for each condition where n=9 mice pooled from 3 independent experiments. Shown as mean ± SEM. Paired t-test was performed, $p < 0.05$. **e**, Heatmap showing relative levels of glycolytic and TCA cycle metabolites extracted from quiescent (Telogen, day 50), activated (Telogen-Anagen, day 70) and HFSCs that have returned to the quiescent state (Anagen, day 90). Data shown were generated from n=3 animals per timepoint in 3 independent experiments.

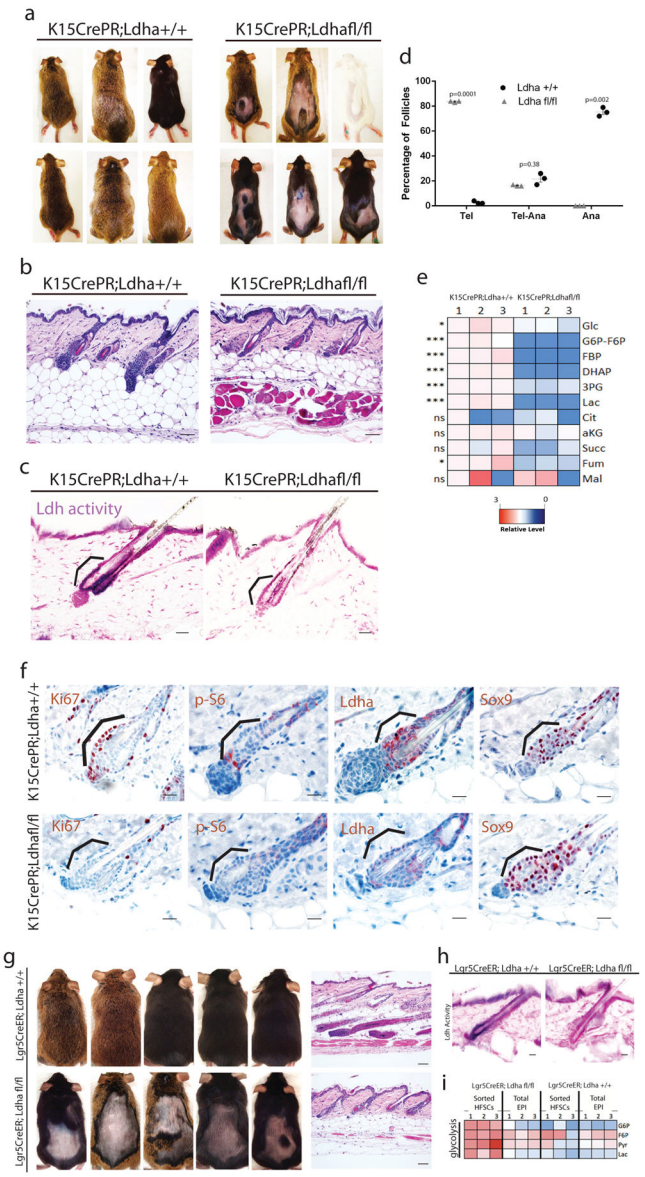

Figure 3. Deletion of Ldha blocks HFSC activation

a, *Ldha*$^{+/+}$ animals enter the hair cycle synchronously around day 70 as measured by shaving and observation beginning at day 50. *K15CrePR;Ldha*$^{fl/fl}$ animals treated with Mifepristone show defects in anagen entry. Results are representative of at least 33 animals of each genotype. **b**, Skin pathology showing that *K15CrePR;Ldha*$^{fl/fl}$ animals showed neither and remained in telogen. Scale bars indicate 50 micrometers. **c**, Ldh enzyme activity assay showed that *K15CrePR;*Ldha fl/fl animals lacked this activity in the HFSCs (indicated by bracket). Scale bars indicate 20 micrometers. **d**, Graph showing percentage of follicles in telogen, telogen to anagen transition and anagen in *K15CrePR;Ldha*$^{+/+}$ mice versus *K15CrePR;Ldha*$^{fl/fl}$ mice (n = 225 follicles from 3 mice per genotype). Shown as mean ± SEM. Paired t-test was performed, $p < 0.05$, **e**, Heatmap showing relative levels of glycolytic and TCA cycle metabolites extracted from *Ldha*$^{+/+}$ HFSCs and *Ldha*$^{fl/fl}$ HFSCs and

measured by LC-MS. Asterisks indicate significant difference in metabolite levels between genotypes. For **e,** paired t-test was performed,* denotes $p < 0.05$, ** denotes $p < 0.01$, *** denotes $p < 0.001$, ns denotes $p > 0.05$, and n=9 mice pooled from 3 independent experiments. **f**, Immunohistochemistry staining for Ki-67, a marker of proliferation is absent in *Ldha*$^{fl/fl}$ HFSCs. Phospo-S6, a marker in HFSCs at the beginning of a new hair cycle, is absent in *Ldha*$^{fl/fl}$ HFSCs. Staining for Ldha protein shows specific deletion in HFSCs. Brackets indicate bulge. Staining for Sox9 shows that HFSCs are still present in *Ldha* deleted niche. Scale bars: 20 micrometers. **g**, Animals with *Ldha* deletion in their HFSCs as controlled by *Lgr5CreER*, show profound defects in the entry into anagen. **right**, Skin pathology showing that *Lgr5CreER;Ldha*$^{fl/fl}$ animals mostly remained in telogen. Scale bars: 100 micrometers. Results are representative of at least 12 animals of each genotype. **h**, Ldh enzyme activity assay in the epidermis shows that *Lgr5CreER;Ldha*$^{fl/fl}$ animals lacked this activity in the HFSCs. Scale bars: 20 micrometers. **i**, LC-MS analysis of metabolites from indicated mice. Data were generated from n=3 animals per condition pooled from 3 independent experiments.

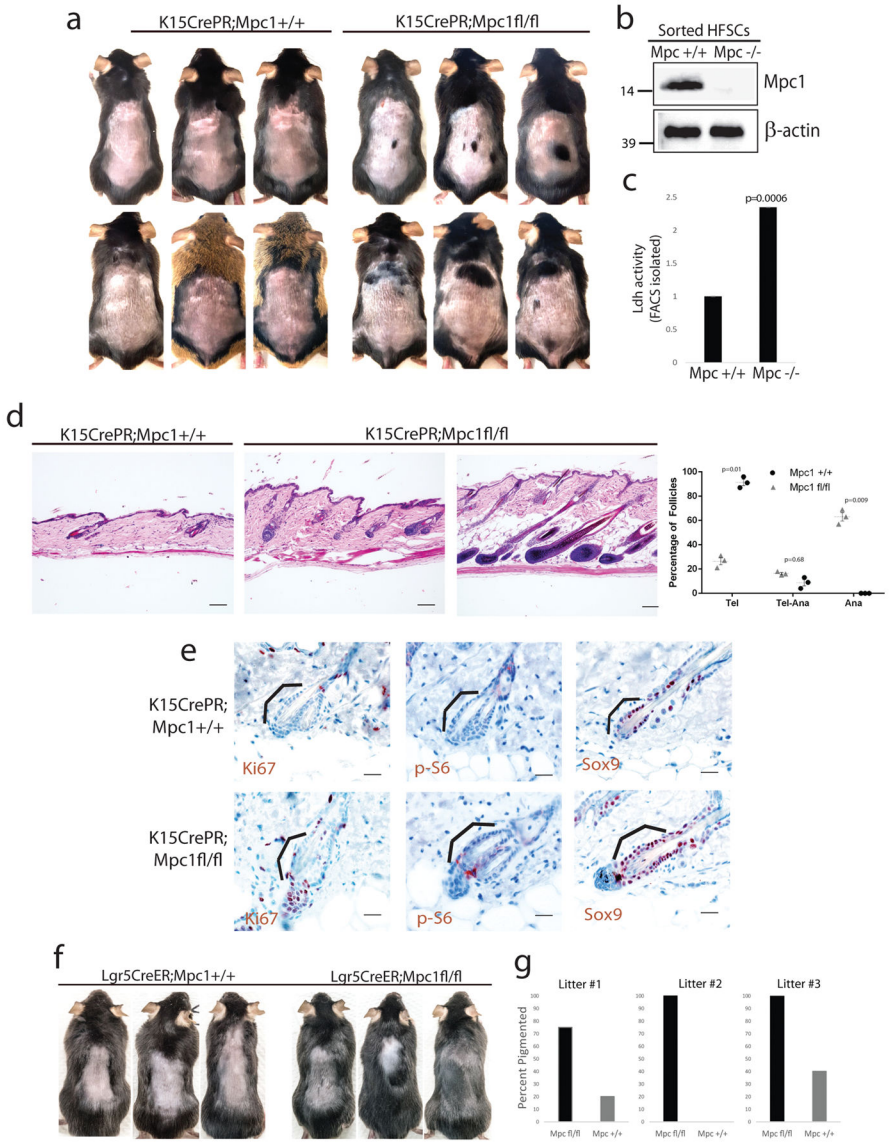

Figure 4. Deletion of Mpc1 increases lactate production and activation of HFSCs

a, Mpc1fl/fl animals show pigmentation and hair growth, consistent with entry into the anagen cycle at 8.5 weeks, whereas Mpc1+/+ animals do not show dorsal pigmentation and hair growth this early. Animals shown are representative of at least 12 animals of each genotype. **b,** FACS isolation of HFSC bulge populations in Mpc1+/+ versus Mpc1fl/fl mice followed by western blotting shows successful deletion of Mpc1 protein in the stem cell niche. β-actin is a loading control. **c,** Plate reader assay for Ldh activity on sorted HFSC populations shows elevated activity in Mpc1fl/fl HFSCs compared to Mpc1+/+ HFSCs. Each bar represents the average signal for each genotype where n=9 mice pooled from 3 independent experiments. Shown as mean ± SEM. Paired t-test was performed, $p < 0.05$. **d,** Histology on WT versus Mpc1 deletion skin shows induction of anagen in absence of Mpc1. Scale bars indicate 100 micrometers. Quantification of phenotype at right shows percentage of dorsal follicles in telogen, telogen to anagen transition and anagen in Mpc1 +/+ mice

versus Mpc1fl/fl mice (n = 250 follicles from 3 mice per genotype). Shown as mean ± SEM. Paired t-test was performed, $p < 0.05$. **e,** Immunohistochemistry staining for Ki-67, a marker of proliferation that is only active in HFSCs at the beginning of a new hair cycle, is only present in Mpc1fl/fl HFSCs at 8.5 weeks, consistent with their accelerated entry into a new hair cycle. Phospo-S6, another marker that is only active in HFSCs at the beginning of a new hair cycle, is only present in Mpc1fl/fl HFSCs. Staining for Sox9 shows that HFSCs are present in Mpc1 deleted niche. Images taken at 60X magnification. **f,** Deletion of Mpc1 in mice bearing the Lgr5CreER allele shows strong induction of the hair cycle. Note that red boxes indicate areas of new hair growth. Results are representative of at least 9 animals per genotype. **g,** Quantification of pigmentation in the indicated genotypes across three independent litters (n = 5 mice per genotype). Unprocessed scans of blots are shown in Supplementary Figure 6.

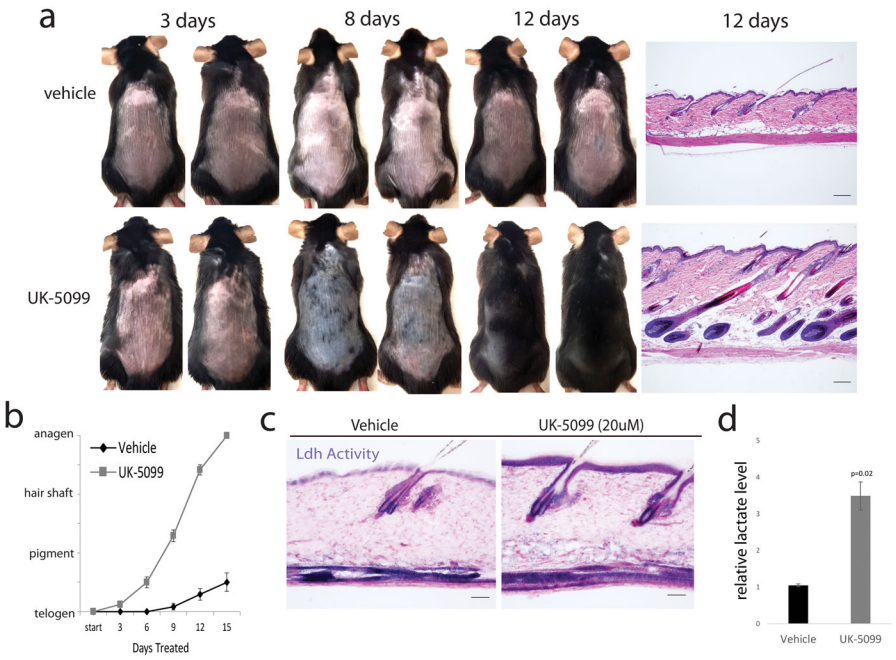

Figure 5. Pharmacological inhibition of Mpc1 promotes HFSC activation

a, Animals treated topically with UK-5099 (20uM) show pigmentation and hair growth, indicative of entry into anagen, after 8 days of treatment. Full anagen, indicated by full coat of hair, is achieved after 14 days of treatment. Mice treated topically with vehicle control do not show pigmentation nor hair growth even after 12 days of treatment. **right**, Skin pathology showing that UK-5099 animals enter an accelerated anagen at 8 weeks typified by down growth of the follicle and hypodermal thickening, while vehicle control treated animals showed neither and remained in telogen. Images shown are representative of at least 14 mice from 7 independent experiments. Scale bars indicate 100 micrometers. **b**, Graph showing time to observed phenotype in vehicle versus UK-5099 treated mice. n = 6 mice per condition. Shown as mean ± SEM. **c**, Ldh enzyme activity assay in the epidermis shows strong activity in HFSCs in vehicle control and UK-5099 treated animals. Ldh enzyme activity also seen in interfollicular epidermis of UK-5099 treated animals. Ldh activity is indicated by purple stain; pink is nuclear fast red counterstain. Scale bars indicate 50 micrometers. **d**, Metabolomic analysis of Lactate on HFSCs isolated from UK-5099 treated skin for 48 hours; Each bar represents the average signal for each condition where n=9 mice pooled from 3 independent experiments. Shown as mean ± SEM. Paired t-test was performed, $p < 0.05$.

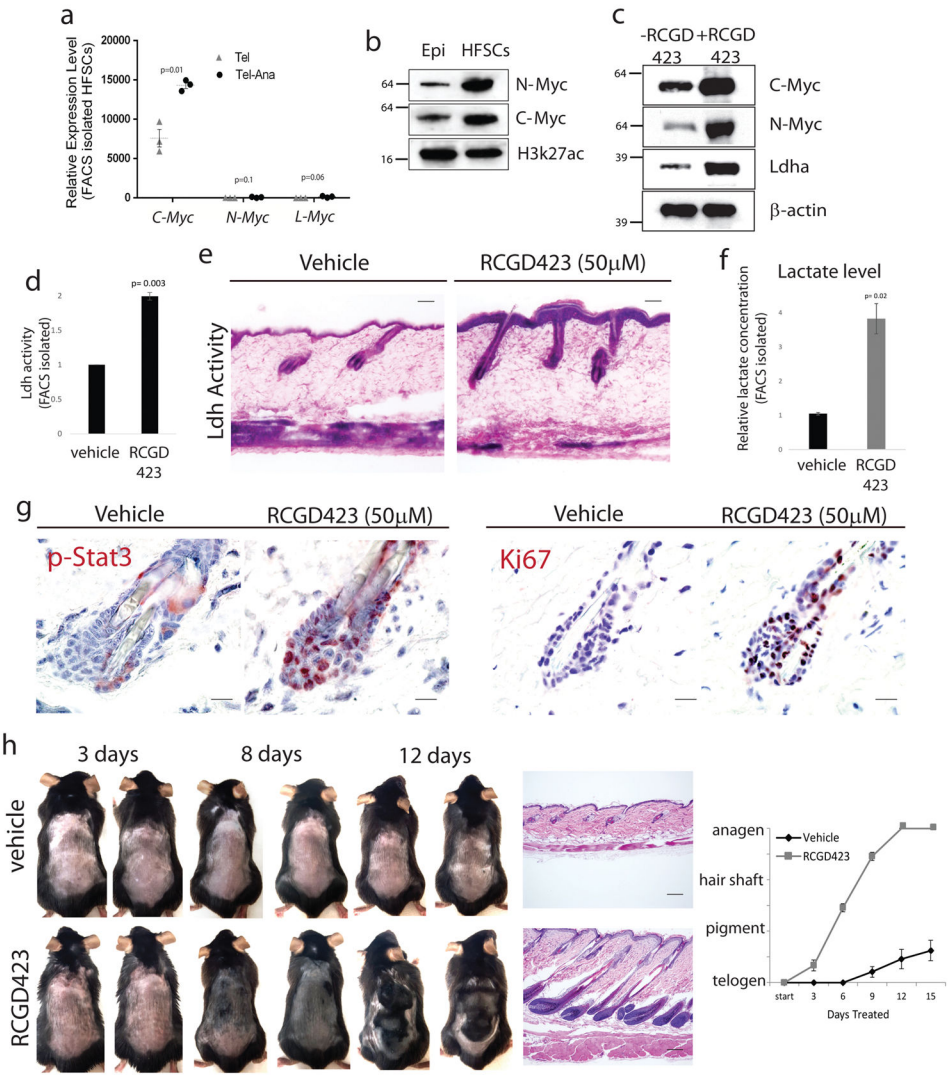

Figure 6. Stimulation of Myc levels promotes HFSC activation

a, RNA-seq data from sorted HFSCs in telogen and telogen-anagen transition[35]. n=3 mice per timepoint. Shown as mean ± SEM. Paired t-test was performed, $p < 0.05$. **b,** Nuclear protein fractions show expression of n-Myc and c-Myc in HFSCs compared to epidermal cells. H3k27ac is a loading control for nuclear proteins. **c,** Total protein preps from skin treated with 2 topical doses of RCGD423 (50uM) show increased c-Myc, n-Myc and Ldha protein levels compared to animals that received 2 topical doses of vehicle control. β-actin is a loading control. **d,** Plate reader assay for Ldh enzyme activity in the epidermis. Each bar represents the average signal for each condition where n=9 mice pooled from 3 independent experiments. Shown as mean ± SEM. Paired t-test was performed, $p < 0.05$. **e,** Ldh enzyme activity assay in the epidermis in vehicle control and RCGD423 treated animals. Scale bar indicates 50 micrometers. **f,** Metabolomic analysis of Lactate on HFSCs isolated from RCGD423 treated skin for 48 hours. Each bar represents the average signal for each condition where n=9 mice pooled from 3 independent experiments. Shown as mean ± SEM. Paired t-test was performed, $p < 0.05$. **g,** Immunohistochemistry staining for Ki-67 and

phospo-Stat3, a downstream marker of RCGD423 activity. Scale bar indicates 20 micrometers. **h,** Animals treated with RCGD423 (50uM) show pigmentation and hair growth, indicative of entry into anagen, after 5 doses. Images shown are representative of at least 14 mice from 7 independent experiments. Scale bar indicates 100 micrometers. Quantification of phenotype showing time to observed phenotype in vehicle versus RCGD423 treated mice. n = 6 mice per condition. Shown as mean ± SEM. Unprocessed scans of blots are shown in Supplementary Figure 6.